

SUPPORTING INFORMATION

Dual-Emission Eu-doped $\text{Ca}_{2-x}\text{Sr}_x\text{PN}_3$ Nitridophosphate Phosphors Prepared by Hot Isostatic Press

Mu-Huai Fang,^{‡a} Hsi-Ping Hsueh,^{‡a} Thangaraji Vasudevan,^a Wen-Tse Huang,^a Zhen Bao,^a Natalia Majewska,^b Sebastian Mahlik,^{b,*} Hwo-Shuenn Sheu,^c and Ru-Shi Liu^{a,*}

^aDepartment of Chemistry, National Taiwan University, Taipei 106, Taiwan

^bInstitute of Experimental Physics, Faculty of Mathematic, Physics and Informatics, Gdańsk University,
Wita Stwosza 57, 80-308 Gdańsk, Poland

^cNational Synchrotron Radiation Research Center, Hsinchu 300, Taiwan

EXPERIMENTAL METHODS

Reagents. Calcium nitride (Ca_3N_2 ; 99.0%), strontium nitride (Sr_3N_2 ; 99.5%), and europium nitride (EuN ; 99.9%) were obtained from Materion. Phosphorus red (P_{red} , 98.9%) was purchased from Alfa Aesar.

Synthesis of $\text{Ca}_{1.94-x}\text{Sr}_x\text{PN}_3:0.06\text{Eu}^{2+}$. Owing to the moisture-sensitive nature of the starting materials, all experiments were carried out in an inert gas-filled glovebox ($\text{O}_2 < 1$ ppm, $\text{H}_2\text{O} < 1$ ppm). The starting materials were mixed in an agate mortar and put into tungsten crucibles, which were then placed in a hot isostatic press (HIP; AIP6-30H, American Isostatic Presses, Inc., Columbus, OH, USA). After heating the sample to 1200 °C at a rate of 20 °C/min under 150 MPa pressure and maintain these conditions for 10 h, the samples were cooled to room temperature (RT) and $\text{Ca}_{1.94-x}\text{Sr}_x\text{PN}_3:0.06\text{Eu}^{2+}$ phosphors were obtained.

Characterization. Synchrotron powder X-ray diffraction patterns of $\text{Ca}_{1.94-x}\text{Sr}_x\text{PN}_3:0.06\text{Eu}^{2+}$ were acquired from the National Synchrotron Radiation Research Center (Taiwan) BL01C2 beamline at room temperature (RT) using a Debye–Scherrer camera. The pattern was used for Rietveld analysis using Total Pattern Analysis Solutions software (TOPAS 4.2). RT photoluminescence (PL) photoluminescence excitation (PLE) spectra were measured with a FluoroMax-4P spectrofluorometer (Horiba) equipped with a 150 W xenon lamp as an excitation source and an R928 Hamamatsu photomultiplier as a detector, which enabled the recording of PL and PLE spectra within the spectral range of 250–850 nm. PL spectra were obtained with an Andor SR-750-D1 spectrometer equipped with a CCD camera (DU420A-OE). A Kimmon Koha He–Cd laser (442 nm) was used as an excitation source. Decay profiles were obtained using time-resolved spectroscopy apparatus equipped with a PG 401/SH optical parametric generator pumped by a PL2251A pulsed YAG:Nd laser (EKSPLA). The detection part consisted of a 2501S grating spectrometer (Bruker Optics) combined with a C4334-01 streak camera (Hamamatsu). Data were recorded in the form of streak images on a 640×480 pixel CCD array. The photon-counting algorithm-based software was used to transform the result into a 2D matrix of photon counts versus wavelength and time (streak image).

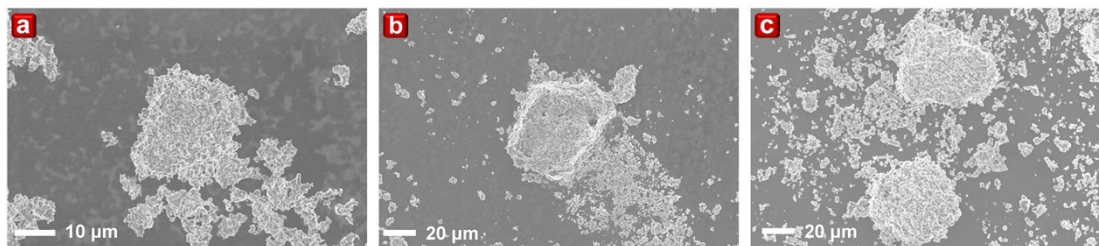


Figure S1. SEM images of $\text{Ca}_{1.94-x}\text{Sr}_x\text{PN}_3:0.06\text{Eu}^{2+}$. (a) $x = 0$, (b) $x = 0.3$, and (c) $x = 0.7$.

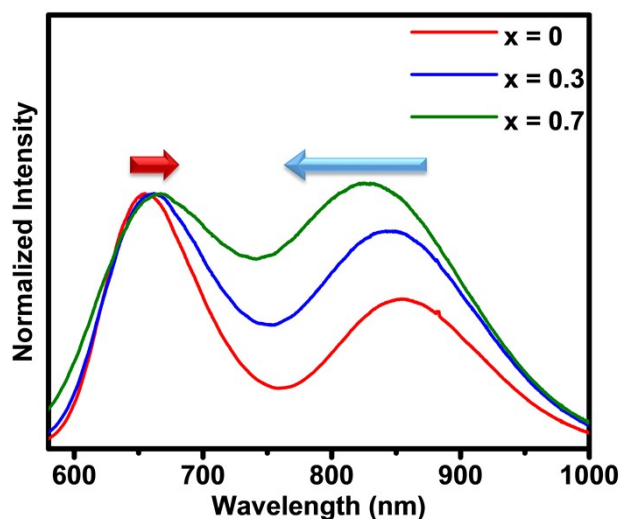


Figure S2. Normalized photoluminescence of $\text{Ca}_{1.94-x}\text{Sr}_x\text{PN}_3:0.06\text{Eu}^{2+}$ ($x = 0, 0.3$, and 0.7)

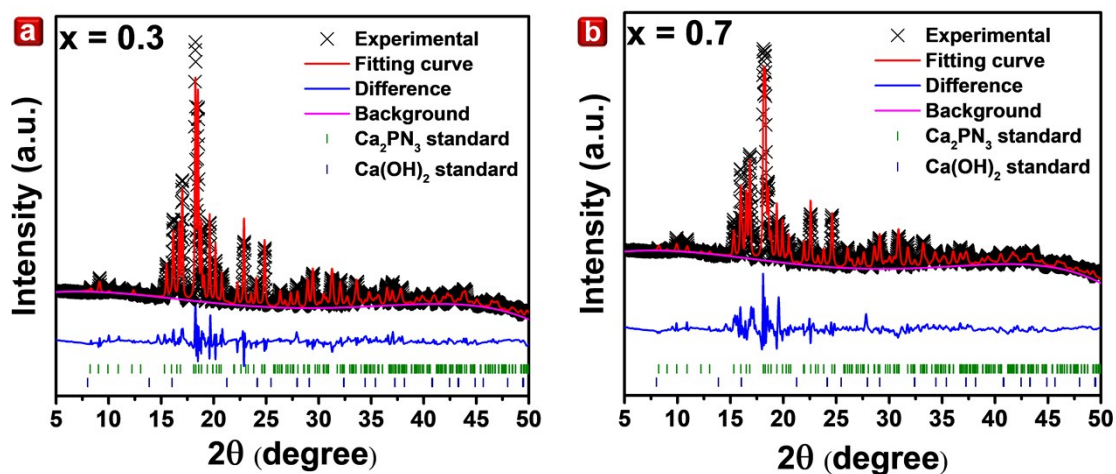


Figure S3. Rietveld refinement patterns of $\text{Ca}_{1.94-x}\text{Sr}_x\text{PN}_3:0.06\text{Eu}^{2+}$. (a) $x = 0.3$ and (b) $x = 0.7$.

Table S1. Internal quantum efficiency of $\text{Ca}_{1.94-x}\text{Sr}_x\text{PN}_3:0.06\text{Eu}^{2+}$.

Samples	Internal Quantum Efficiency (%)
x = 0	6.9
x = 0.3	6.7
x = 0.7	5.6

Table S2. Lattice parameters and atomic positions derived from the Rietveld refinement of $\text{Ca}_{1.94}\text{PN}_3:0.06\text{Eu}^{2+}$.

Crystal system		Orthorhombic			
Space group	<i>Cmce</i>	<i>a</i>	5.19212(20) Å		
<i>Rwp</i>	9.54%	<i>b</i>	10.31942(43) Å		
<i>Rp</i>	6.85%	<i>c</i>	11.30808(45) Å		
χ^2	2.67	<i>V</i>	605.883(42) Å ³		

Atoms	x	y	z	Occ	Beq (Å ²)
Ca1	0	0.05141(34)	0.35863(34)	1	1.126(90)
Ca2	0	0.36173(28)	0.42619(29)	1	1.126(90)
P1	0	0.24519(45)	0.16606(43)	1	0.93(12)
N1	0	0.3383(11)	0.0540(11)	1	0.97(15)
N2	0	0.0921(12)	0.1418(12)	1	0.97(15)
N3	0.25	0.2872(12)	0.25	1	0.97(15)

Table S3. Lattice parameters and atomic positions derived from the Rietveld refinement of $\text{Ca}_{1.64}\text{Sr}_{0.3}\text{PN}_3\cdot 0.06\text{Eu}^{2+}$.

Crystal system	Orthorhombic				
Space group	<i>Cmce</i>	<i>a</i>	5.20615(55) Å		
<i>Rwp</i>	12.42%	<i>b</i>	10.3705(11) Å		
<i>Rp</i>	9.58%	<i>c</i>	11.3673(12) Å		
χ^2	3.45	<i>V</i>	613.73(11) Å ³		

Atoms	x	y	z	Occ	Beq (Å ²)
Ca1	0	0.05330(42)	0.35651(40)	0.8515(64)	0.44(12)
Sr1	0	0.05330(42)	0.35651(40)	0.1485(64)	0.44(12)
Ca2	0	0.35781(36)	0.42561(36)	0.8485(64)	2.32(14)
Sr2	0	0.35781(36)	0.42561(36)	0.1515(64)	2.32(14)
P1	0	0.23715(55)	0.16654(56)	1	0.50(15)
N1	0	0.3500(17)	0.0699(18)	1	3.01(23)
N2	0	0.0847(18)	0.1415(18)	1	3.01(23)
N3	0.25	0.2880(19)	0.25	1	3.01(23)

Table S4. Lattice parameters and atomic positions derived from the Rietveld refinement of $\text{Ca}_{1.24}\text{Sr}_{0.7}\cdot 0.06\text{Eu}^{2+}$.

Crystal system	Orthorhombic				
Space group	<i>Cmce</i>	<i>a</i>	5.25086(90) Å		
<i>Rwp</i>	14.52%	<i>b</i>	10.5227(19) Å		
<i>Rp</i>	10.32%	<i>c</i>	11.5411(19) Å		
χ^2	4.27	<i>V</i>	637.68(19) Å ³		

Atoms	x	y	z	Occ	Beq
Ca1	0	0.05134(49)	0.35623(47)	0.4806(84)	1.00(15)
Sr1	0	0.05134(49)	0.35623(47)	0.5194(84)	1.00(15)
Ca2	0	0.35653(51)	0.42573(49)	0.8194(84)	1.40(19)
Sr2	0	0.35653(51)	0.42573(49)	0.1806(84)	1.40(19)
P1	0	0.23812(82)	0.16690(85)	1	0.56(23)
N1	0	0.3511(24)	0.0713(23)	1	2.49(34)
N2	0	0.0890(26)	0.1475(24)	1	2.49(34)
N3	0.25	0.2747(23)	0.25	1	2.49(34)

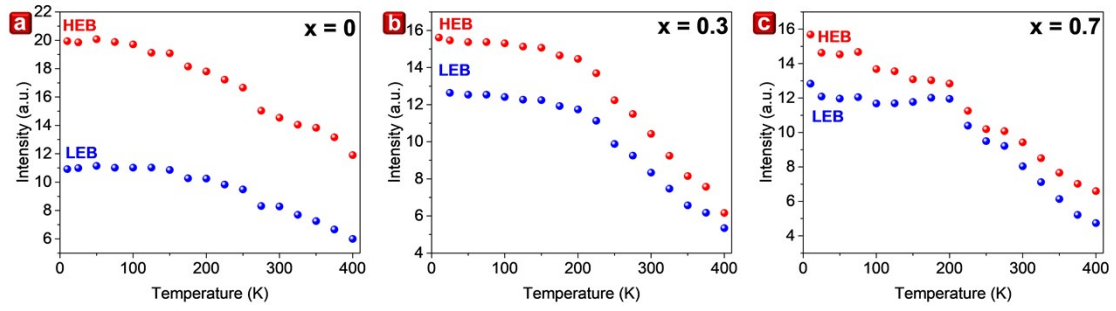


Figure S4. Temperature-dependent PL of the HEB and LEB of $\text{Ca}_{1.94-x}\text{Sr}_x\text{PN}_3:0.06\text{Eu}^{2+}$. (a) $x = 0$, (b) $x = 0.3$, and (c) $x = 0.7$.

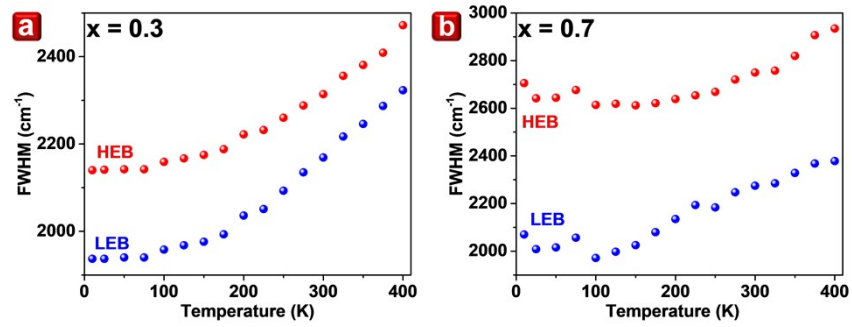


Figure S5. Temperature-dependent FWHM of the HEB and LEB of $\text{Ca}_{1.94-x}\text{Sr}_x\text{PN}_3:0.06\text{Eu}^{2+}$. (a) $x = 0.3$ and (b) $x = 0.7$.

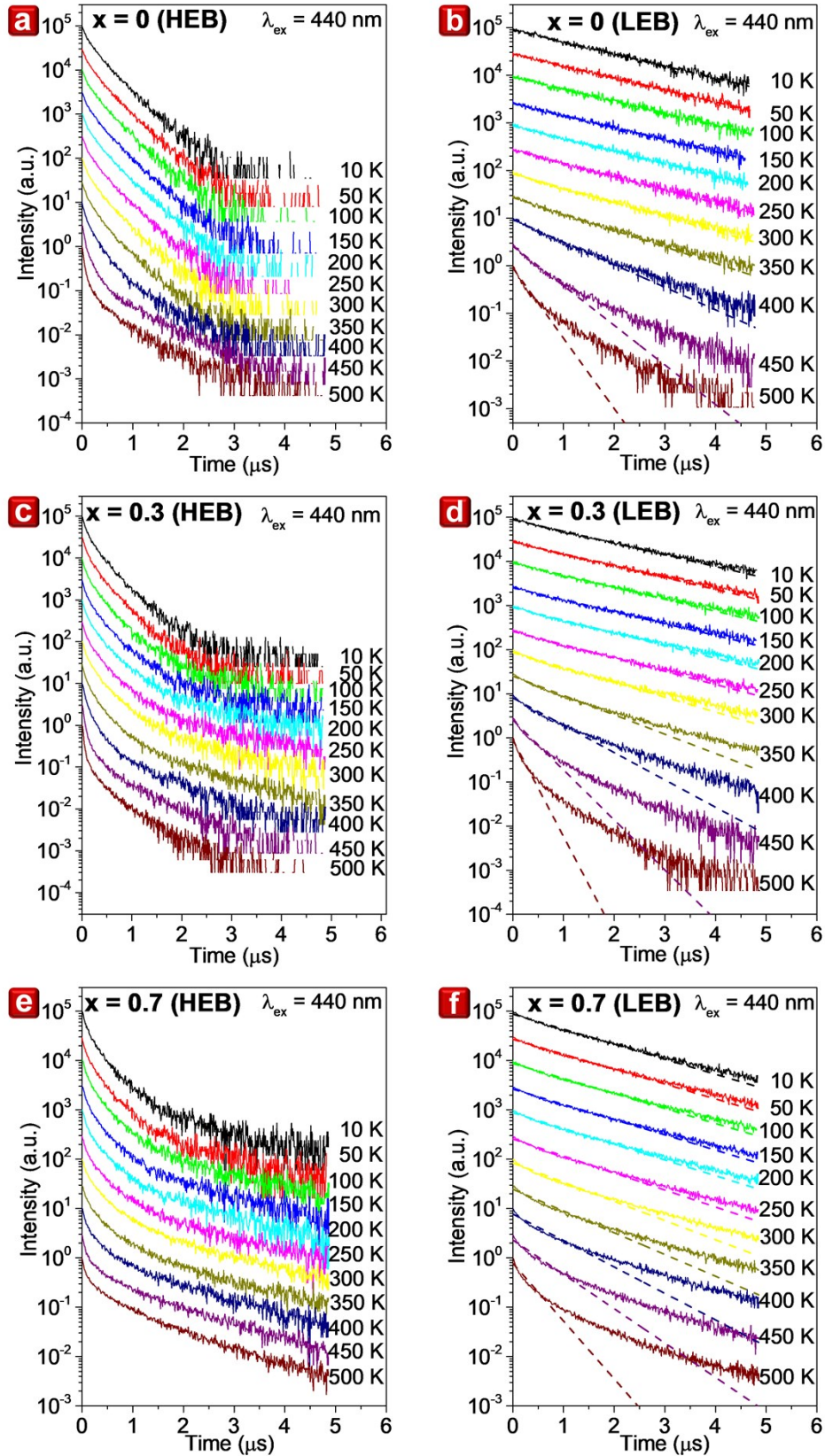


Figure S6. Temperature-dependent decay profiles of $\text{Ca}_{1.94-x}\text{Sr}_x\text{PN}_3:0.06\text{Eu}^{2+}$. (a) $x = 0$ (HEB), (b) $x = 0$ (LEB), (c) $x = 0.3$ (HEB), (d) $x = 0.3$ (LEB), (e) $x = 0.7$ (HEB), and (f) $x = 0.7$ (LEB).

Thermal-stability analysis:

The decay-time calculation of HEB luminescence is unreliable because of multi-exponential behavior and overlapping at high temperatures with luminescence from the LEB. The non-exponential decay of HEB may be evidence of energy transfer from Eu^{2+} (HEB) to Eu^{2+} (LEB). However, any temperature dependence of this process is difficult to determine. By contrast, using LEB emission can enable the calculation of decay times by fitting the experimental data into the following formula:

$$I(t) = I_0 e^{-\frac{t}{\tau}} \quad (\text{s1})$$

where $I(t)$ is emission intensity at time t , I_0 is the initial intensity, and τ is the decay time of the luminescence. The calculated decay times at different temperatures for all samples are presented in Figure S7. Notably, at high temperatures, the decays of LEB become non-exponential. In addition to the shorter decay component, a long decay component exists possibly due to additional thermally activated processes such as the release of electrons from electron traps. The calculated decay times are constant below 150 K for the three samples and shorten with increased temperature. The temperature-dependent decay times for $\text{Ca}_{1.94-x}\text{Sr}_x\text{PN}_3:0.06\text{Eu}^{2+}$ ($x = 0, 0.3, \text{ and } 0.7$) do not exhibit the typical behavior of a system with one non-radiative process. A very good interpretation of the data in Figure S7 is achieved using two nonradiative pathways, defined by the non-radiative rates p_{nr1} and p_{nr2} , and the respective activation energies E_{A1} and E_{A2} . The temperature-dependent decay time is given by the following formula:¹

$$\tau(T) = \frac{1}{\frac{1}{\tau_0} + p_{nr1} \exp\left(-\frac{E_{A1}}{kT}\right) + p_{nr2} \exp\left(-\frac{E_{A2}}{kT}\right)} \quad (\text{s2})$$

The parameters obtained from fitting using formula (s2) are listed in Figures S7a–S7c. From the calculation, we obtain one pathway characterized by E_{A1} (2760–3150 cm^{-1}) and high probability (10^{10} s^{-1}) and a second one with a lower activation energy E_{A2} (550–660 cm^{-1}), as well as the corresponding lower probability (10^6 s^{-1}). The pathway characterized by higher activation energy and higher probability can be related to the autoionization of Eu^{2+} , considered as the transition from $4f^65d^1$ to the conduction band. The pathway with lower non-radiative activation energy and probability can be

related to the non-radiative energy transfer between two different Eu^{2+} crystallographic centers.²

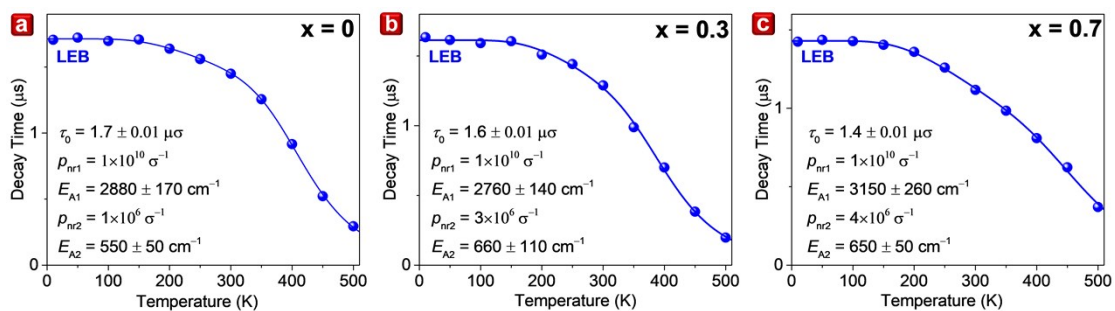


Figure S7. Temperature-dependent decay profiles of $\text{Ca}_{1.94-x}\text{Sr}_x\text{PN}_3:0.06\text{Eu}^{2+}$. (a) $x = 0$, (b) $x = 0.3$, and (c) $x = 0.7$.

References:

1. M. Grinberg and W. Jaskólski, *Phys. Rev. B* 1997, **55**, 5581.
2. A. Lazarowska, S. Mahlik, M. Grinberg, C. W. Yeh and R. S. Liu, *Opt. Mater.* 2014, **37**, 734–739.